Asymmetric molecular-orbital tomography by manipulating electron trajectories

Bincheng Wang,[1] Qingbin Zhang,[1,*] Xiaosong Zhu,[1,†] Pengfei Lan,[1] Seyed Ali Rezvani,[1] and Peixiang Lu[1,2]

[1]*School of Physics and Wuhan National Laboratory for Optoelectronics, Huazhong University of Science and Technology, Wuhan 430074, China*

[2]*Laboratory of Optical Information Technology, Wuhan Institute of Technology, Wuhan 430205, China*

We present a scheme for tomographic imaging of asymmetric molecular orbital based on high-order harmonic generation with a two-color orthogonally polarized multicycle laser field. With the two-dimensional manipulation of the electron trajectories, the electrons can recollide with the target molecule from two noncollinear directions, and then the dipole moment generated from the single direction can be obtained to reconstructed the asymmetric molecular orbital. The recollision is independent from the molecular structure and the angular dependence of the ionization rate in the external field. For this reason, this scheme can avoid the negative effects arising from the modification of the angle-dependent ionization rate induced by Stark shift and be applied to various molecules.

I. INTRODUCTION

High-order harmonic generation (HHG) is known as a promising tabletop source of the attosecond extreme-ultraviolet radiation for various applications in strong field physics [1,2]. The dynamics of HHG can be described by the three-step model: (1) the electron is ionized by a strong laser field [3], (2) the electron is accelerated in the laser field [4,5], and (3) the accelerated electron recombines with the parent ion and the high-order harmonic is generated [6]. The generated high-order harmonic can be used to acquire the attosecond pulse. At the same time, the recombination of electron with the parent ion during HHG ensures that the structure and internal dynamics of the radiating atoms or molecules are encoded in the harmonic spectra [7–15]. One of the methods used to probe the molecular structure is molecular orbital tomography, which was first proposed by Itatani to reconstruct the highest occupied molecular orbital (HOMO) of N_2 [16]. Since then, molecular orbital tomography has attracted a great deal of attention for its great significance in uncovering the molecular orbital structure [17–20]. In order to reconstruct molecular orbital, one has to record the harmonic spectra for different molecular orientations and extract the structure information of the target orbital from the harmonic spectra. However, in a linearly polarized laser field, free electrons recollide with the parent molecule from two opposite directions of the molecule, and therefore, the target's orbital information obtained from the two directions are coupled in each order harmonic. For molecules with symmetric molecular orbital such as CO_2 [19], the orbital information of the two directions is the same and distinguishable. However, most molecules are asymmetric, and the asymmetric molecular orbital tomography (AMOT) is more complicated. For an asymmetric molecule, the information coupled in the harmonic spectra is fundamentally different and undeterminable; thus the electrons should be controlled to recollide from only one direction to decouple the orbital information. Then the dipole

moment which contains the unidirectional orbital information can be used to achieve the AMOT.

Elmar *et al.* proposed that a single-cycle pulse with a stable and controllable carrier-envelope phase can achieve the unidirectional recollision [21]. To achieve the unidirectional recollision in the experiment, a scheme with a collinear two-color multicycle laser field had also been proposed [22]. Both of these schemes apply the exponential dependence of the tunneling ionization rate on the amplitude of the electric field to carry out the unidirectional recollision. Due to the exponential dependence of the tunneling ionization rate on the amplitude of electric field, the electrons are dominantly ionized from one side and then recollide from the same side. However, using the relationship between ionization rate and the amplitude of electric field to implement the unidirectional recollision has a limitation. When molecules interact with the strong laser field, a Stark shift will occur and the energy levels of molecule will be changed. For the molecules with large permanent dipole, this non-negligible Stark shift of the orbital energy will have an influence on the molecular orbital tomography [23]. The Stark shift of the orbital energy can efficiently modify the angular dependency of the ionization rate. This leads to the comparable ionization probabilities from both directions of the electric field and under these circumstances, the unidirectional recollision condition is no longer guaranteed and the AMOT is no longer feasible. For this reason, a scheme which is independent from the ionization is necessary. High-order harmonic generation has three steps: (1) ionization, (2) acceleration, and (3) recollision. Apart from controlling the ionization step, the manipulation of electron motion in the acceleration step is a more straightforward method to satisfy the unidirectional recollision condition. The recent researches in this field have shown that two-color orthogonally polarized laser fields can be used to control the electron motion [4,5]. This method can be used in different applications such as probing the molecular orbital [24,25] and imaging molecular motion [26,27].

In this paper, we propose a scheme of AMOT based on the 2D manipulation of the electron trajectories with a two-color orthogonally polarized multicycle laser field. In the two-color orthogonally polarized laser field, the electrons are manipulated to recollide with the parent molecule from

---

*zhangqingbin@hust.edu.cn

†zhuxiaosong@hust.edu.cn

two noncollinear directions, which is independent from the ionization. The recollision depends only on the electric field. No matter how the ionization rate is dependent on the angle between the instantaneous electric field direction and the molecular axis, the electrons always return to the parent molecule in two noncollinear directions. Then we demonstrate that by exploiting the relationship between the dipole moment and the recollision angle, the dipole moment generated from the single direction can be obtained and the unidirectional recollision condition could be satisfied in this scheme. It is worth noting that our method is based on the manipulation of the acceleration process to realize the unidirectional recollision, which is essentially different from the methods used in previous works. Manipulating electrons' motion provides a straightforward way to carry out molecular orbital tomography. It can be used not only to avoid the problem that molecular orbital cannot be imaged under the Stark effect, but also extends the molecular orbital tomography to both asymmetric and symmetric molecules. Moreover, the two-color orthogonally polarized laser field has been widely used in experiments [5,24,25,27], thus our scheme based on the two-color orthogonally polarized multicycle laser field can also be easily implemented in experiments.

II. CLASSICAL ANALYSIS

To analyze the 2D trajectories of the electrons in two-color orthogonally polarized laser field, we use the semiclassical model to calculate the trajectories. The evolution of the electron (ionized at t_0) is described by the following classical equations:

$$\frac{d^2\mathbf{r}}{dt^2} = -\mathbf{E}(t), \quad \dot{\mathbf{r}}_x(t_0) = -p_0 \sin(\theta_E),$$

$$\dot{\mathbf{r}}_y(t_0) = p_0 \cos(\theta_E), \quad \mathbf{r}(t_0) = 0, \tag{1}$$

where the p_0 is the initial perpendicular momentum of the electron and ranges from -5 to 5 a.u. θ_E is the angle between $-\mathbf{E}(t_0)$ and the x axis. The initial distribution of the electron momentum is taken into account to simulate the spreading of electron wave packet. When the electron approaches the parent ion within a distance of 1 a.u, the recollision is judged and the each recollision electron is weighted by [28]

$$w(t_0, w_0) = w_1(t_0)\, w_2(p_0), \tag{2}$$

where w_1 is the tunnel ionization rate at different initial time t_0 and calculated within the molecular ADK model (MO-ADK model) for an oriented CO molecule [29,30], and

$$w_2(p_0) = \exp\left[\frac{-\sqrt{2I_p}\, p_0^2}{\sqrt{E_x^2 + E_y^2}}\right], \tag{3}$$

where I_p is the ionization energy. Finally, the weighted number of recollision electrons is counted to analyze the distribution of the recollision angles.

An 800 nm fundamental linearly polarized pulse and a 400 nm second-harmonic orthogonally linearly polarized pulse are used to combine the two-color laser field. The intensity of the 800 nm laser is 3×10^{14} W/cm^2 and the 400 nm laser intensity is 3×10^{13} W/cm^2. For simplicitythis laser field is called a $800 + 400$ nm two-color orthogonally polarized laser field. The envelope is trapezoid with the total pulse duration of 14 cycles with two cycles on and off. Figures 1(a)–1(c) are the electric fields corresponding to the different relative phases 0, 0.15π, and 0.3π. Figures 1(d)–1(f) are the corresponding electron trajectories in laboratory frame (x', y'). The results demonstrate that the electrons are manipulated to oscillate in the laser field and then recollide with the parent molecule from two noncollinear directions. The two noncollinear directions correspond to two different groups of trajectories. The colors of the lines in Figs. 1(d)–1(f) denote the corresponding
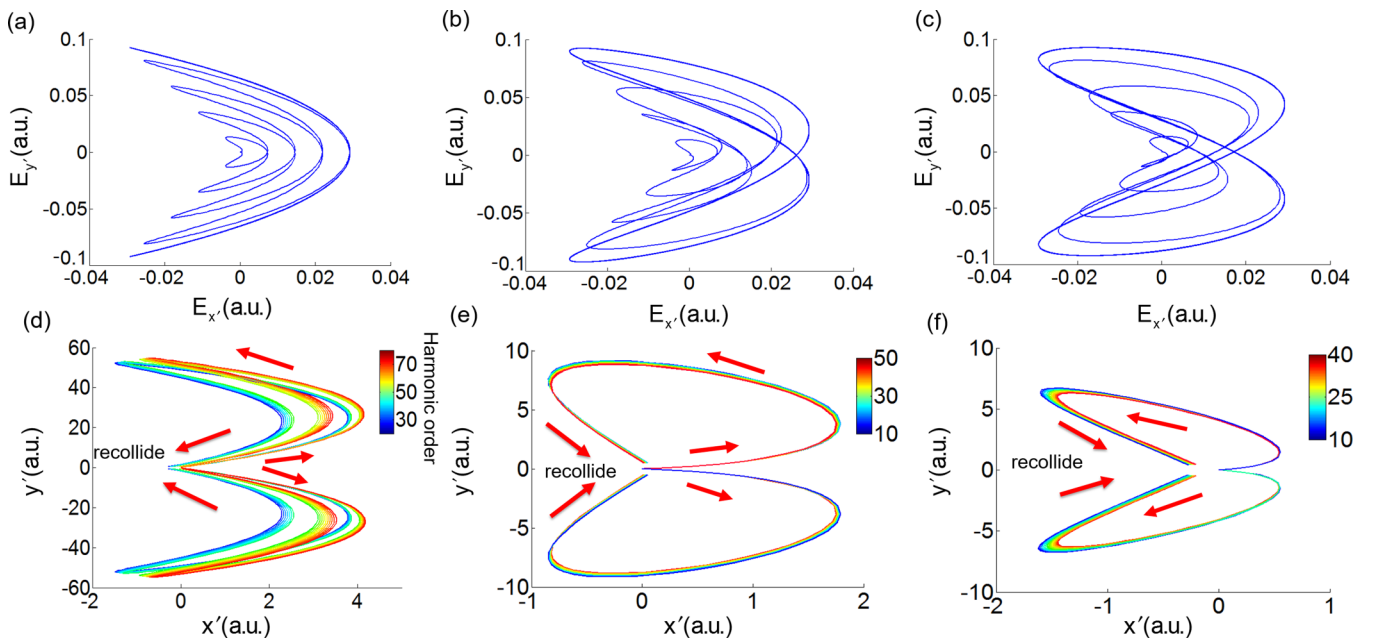

FIG. 1. The electron trajectories in the two-color orthogonally polarized field. (a–c) The electric field corresponding to the different relative phases: 0, 0.15π, and 0.3π. (d–f) The corresponding electron trajectories.
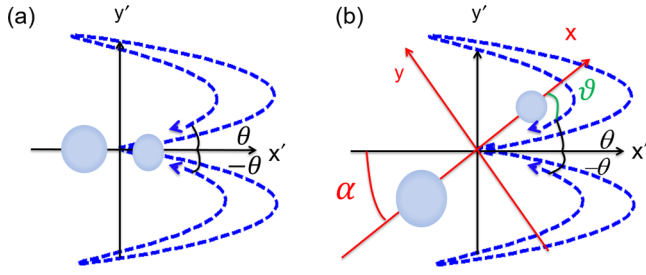
FIG. 2. Schematic of molecular orbital tomography in the two-color orthogonally polarized laser field. (a) Electrons recollide with the parent molecule at angle θ and $-\theta$ in the laboratory frame (x',y'). (b) While the molecule is oriented at angle α, the recollision angle θ stays unchanged.

harmonic orders. It is shown that all the harmonics in a plateau have the same recollision direction. Figures 1(d)–1(f) suggest that the two-color orthogonally polarized laser field can not only perform a 2D manipulation of the electrons but also realizes the special direction recollision among a broad spectral range. The shapes of the electron trajectories are dependent on the relative phases of electric fields. For the different relative phases of electric fields, both the trajectories and the recollision directions are different. In Fig. 1(d) the trajectories are longest, and thus the electrons have the maximum recollision energy. To acquire broad spectral range, the electric field of Fig. 1(a) is chosen to carry out AMOT.

In the two-color orthogonally polarized laser field, the trajectories are dependent only on the electric fields. Figure 2 is a schematic of molecular orbital tomography in the two-color orthogonally polarized laser field. (x,y) are the molecular frame and (x',y') are the laboratory frame. α is the orientation angle of the molecule, and θ is the recollision angle of the electron in the laboratory frame. ϑ is the recollision angle in the molecular frame. As the angle between the molecular frame and the laboratory frame is α, the relationship between these three angles is $\vartheta + \theta = \alpha$ [see Fig. 2(b)]. The recollision angle θ is independent of the molecular orientation angle in the laboratory frame. In order to demonstrate this, θ is calculated in all orientation angles. Figure 3(a) shows the recollision angle [θ and $-\theta$ in Fig. 2(b)] distribution while the molecule is oriented at 45° and Fig. 3(c) exhibits the peak of the recollision angle distribution when the molecule is oriented from 0° to 180°. The top part of Fig. 3(c) corresponds to the recollision angle θ in Fig. 2(b), and the down part is the recollision angle $-\theta$ accordingly. The full width at half maximum (FWHM) of the recollision angle distribution when the molecule is oriented from 0° to 180° is plotted in Fig. 3(d). The top section of Fig. 3(d) is correspondent to the recollision angle θ in Fig. 2(b), and the down section depicts the recollision angle $-\theta$. From Figs. 3(a) and 3(d), it is found that the recollision angles are concentrated around $-14°$ and 14°, and the FWHM of the distribution is approximately 6°. This is because the intensity ratio of the two-color laser field components we used to reconstruct the molecular orbital is 10:1. Therefore the laser field along x' is weak, and it can be regarded as a perturbation for the y' component. As a result, the electrons can be manipulated to recollide with parent molecule in a narrow angle distribution. The FWHM
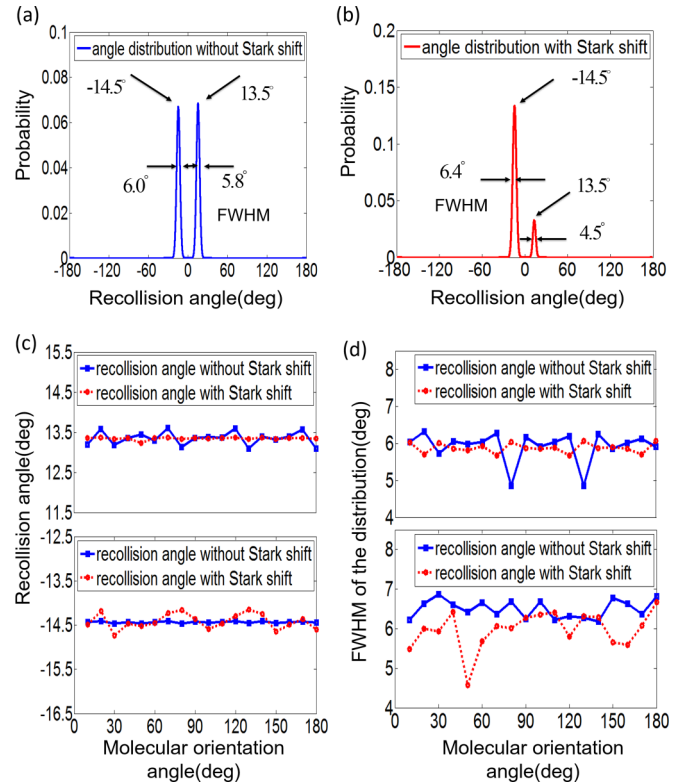

FIG. 3. (a) The recollision angle distribution while the molecule is oriented at 45°. (b) The recollision angle distribution when the Stark shift is considered. (c) The peak of the recollision angle distribution when the molecule is oriented from 0° to 180°. (d) The full width at half maximum (FWHM) of the recollision angle distribution when the molecule is oriented from 0° to 180°.

of the distribution is small and acceptable for the requirement of molecular orbital tomography. In addition, for molecules with large dipole moment, the Stark shift is a nonignorable effect in molecular orbital tomography. The Stark shift can be taken into consideration in the simulation, and the ionization potential becomes time-dependent in response to the external laser field [23] :

$$ I_p(t) = I_{p0} + \vec{\mu} \cdot \vec{F}(t). \qquad (4) $$

I_{p0} is the field free ionization energy, $\vec{\mu}$ is permanent dipole of CO, and $\vec{F}(t)$ is the external electric field. The corresponding results are displayed in Figs. 3(b)–3(d). These results show that when the Stark shift is considered, these above conclusions are still unchanged. The semiclassical analyze suggests that the two-color orthogonally polarized laser field can force the electrons to recollide with parent molecule from two fixed noncollinear directions in the laboratory frame for all orientation angles. These results suggest that our method can be effectively used for AMOT.

III. MOLECULAR ORBITAL TOMOGRAPHY

In the following, we use the laser field shown in Fig. 1(a) to demonstrate the reconstruction of the HOMO of CO. The high-order harmonic spectra of CO are calculated with the SFA model [31]. To demonstrate our scheme can avoid the negative

effect of the Stark shift, the Stark shift is taken into account in the calculation [32]. The ionization energy is replaced by the time-dependent one as shown in Eq. (3). Furthermore, when the recombination process occurs, the electron is already accelerated by the Coulomb potential. Therefore the kinetic energy of the electron is the sum of the energy obtained from the laser field ($k^2/2$) and the potential energy (I_p). To take this acceleration effect into account, a modification should be applied that the momentum k of the recollision electron at the instant of recombination is replaced by the effective momentum k_{eff} [23,33]:

$$k_{\text{eff}} = \sqrt{[k^2 + 2I_p\gamma(k)]}\frac{k}{|k|}. \tag{5}$$

The factor $\gamma(k)$ is given by

$$\gamma(k) = \begin{cases} 1 & k^2 \geqslant I_p \\ \sin^2\left(\frac{\pi k^2}{2I_p}\right) & k^2 < I_p \end{cases}.$$

This k-dependent factor $\gamma(k)$ avoids the unreasonable fact that all the return electrons have momenta larger than $\sqrt{2I_p}$. The introduction of $\gamma(k)$ also suppresses the strong background noises resulting from the jump of k_{eff} over the gap from $-\sqrt{2I_p}$ to $\sqrt{2I_p}$.

The obtained high-order harmonic spectra are shown in Fig. 4. Figures 4(a) and 4(b) show the x' and y' components of the harmonic spectra when molecule is oriented at $45°$. One can see that the cutoff is at about the 80th order. Figure 4(c) shows the x' component of the harmonic spectra when a molecule is oriented from $-5°$ to $-210°$ (this range is used for the reconstruction as discussed below). Figure 4(d) shows the y' component of the harmonic spectra. It is shown that the x' component of the harmonics are suppressed at $-90°$ and the y' component of the harmonic are suppressed at $-180°$. This is because, when a molecule is oriented at $-180°$, the molecular axis is perpendicular to the y' component of the laser field and the ionization is suppressed [34,35]. For the condition that the molecule is oriented at $-90°$, the molecular axis is perpendicular to the x' component of the laser field. As a result, the x' component of the harmonics are suppressed. Also, it is found that when the molecule is oriented at $-180°$, there are only odd harmonics in the y' component and only even harmonics in the x' component. As discussed in Fig. 2, in the x' component, the electrons always recollide with parent molecule from the $+x'$ direction. According to the Eq. (1) in Ref. [5], the harmonics in the x' component have both the odd and even harmonic orders of the 400 nm field, i.e., there are only even harmonics of the 800 nm field. For the y' component, Fig. 2(b) shows that the electrons always recollide in two symmetric directions. Meanwhile the molecule is also symmetric in the y' component, and therefore the harmonics in the y' component have only the odd orders. At $-90°$, the molecular orbital is asymmetric along the y' axis, so there are both odd and even harmonics in the y' component [20]. In the x' component, the HHG is suppressed, and the spectrum is irregular. When the molecule is oriented at other angles except $-180°$ and $-90°$, there are both odd and even harmonics in the x' and y' components. Even harmonics appear in the y' component because the molecular orbital becomes asymmetric along the y' axis. For the x' component, since the molecular
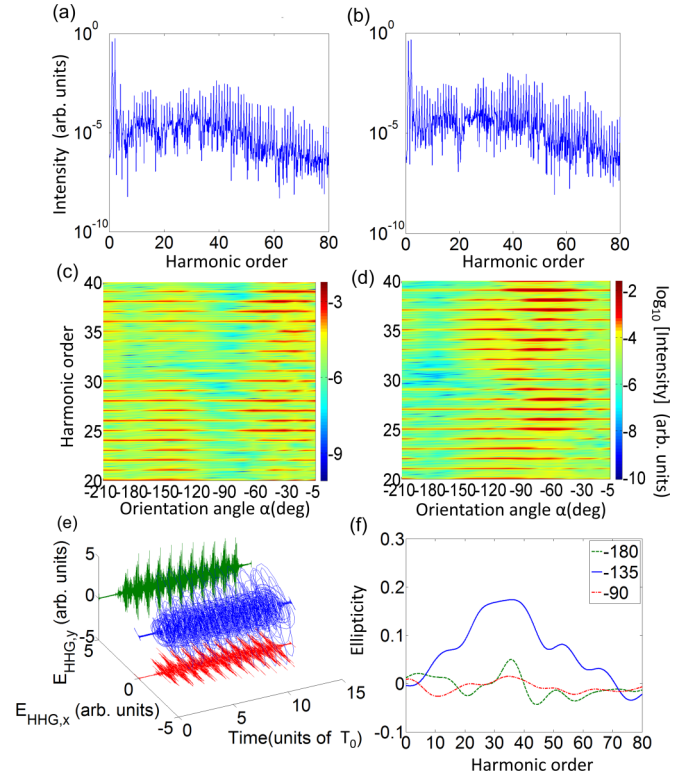

FIG. 4. (a) The x' component of the harmonic spectra when a molecule is oriented at $45°$. (b) The y' component of the harmonic spectra when a molecule is oriented at $45°$. (c) The x' component of the harmonic spectra when a molecule is oriented from $-5°$ to $-210°$. (d) The y' component of the harmonic spectra. (e) The pulse generated by synthesizing the harmonics from H21 to H65 for the orientation angle is $-135°$ (T_0 is the optical cycle of the laser field). (f) The ellipticities of the harmonics when a molecule is oriented at $-90°$, $-135°$, and $-180°$.

axis is neither perpendicular nor parallel to the y' aixs, the y' component of the driving field will contribute odd harmonics to the x' component.

Moreover, in the two-color orthogonally polarized laser field, the harmonics are not always linearly polarized. Figure 4(e) shows the obtained pulse by synthesising the harmonics from H21 to H65 when the molecule is oriented at $-135°$ [2]. It is shown that the generated high-order harmonics are elliptically polarized. The ellipticity of this pulse is plotted in Fig. 4(f). One can see that the ellipticity is up to 0.2. When the orientation angle is close to $-90°$ or $-180°$, the x' or y' component of HHG perpendicular to the molecular axis is suppressed, and the high-order harmonics tends to be linearly polarized. For example, the harmonic ellipticities corresponding to $\alpha = -90$ or -180 are shown in Fig. 4(f). The ellipticities are approximately 0.

In molecular orbital tomography, analogous to the SFA-ansatz the high-order harmonics are generated by the transition from the continuum state to ground state and can be described as [7,14]

$$\vec{E}_{\text{HHG}} = \sum_{\theta} A(\omega,\theta)\,\vec{d}(\omega,\theta). \tag{6}$$

$\vec{E}_{\text{HHG}}$ is the high-order harmonics, $A(\omega,\theta)$ is the complex amplitude of recollision electron wave packet, and $\vec{d}(\omega,\theta)$ is the transition dipole moment. $\vec{E}_{\text{HHG}}$ is contributed by the electrons recolliding with parent molecule from different recollision angles θ. In a linearly polarized laser field, the recollison angles are 0 and π. Thus Eq. (5) is reduced to the general form

$$\vec{E}_{\text{HHG}} = A(\omega,0)\,\vec{d}(\omega,0) + A(\omega,\pi)\,\vec{d}(\omega,\pi). \qquad (7)$$

In our scheme, the electrons are manipulated to recollide with the parent molecule from two noncollinear directions, and in this condition the high-order harmonics can be described as

$$\vec{E}_{\text{HHG}} = A(\omega,\theta)\,\vec{d}(\omega,\theta) + A(\omega,-\theta)\,\vec{d}(\omega,-\theta). \qquad (8)$$

Here $\vec{d}(\omega,\theta)$ and $\vec{d}(\omega,-\theta)$ are the transition dipole moment from the continuum state to ground state corresponding to the recollision angles θ and $-\theta$. For the continuum state, as the spatial scale of the recollision electron wave packet (about 24.47 Å [36]) is larger than the target molecule, it can be regarded as a plane wave [7,16]. Thus, the dipole moment can be extracted with the harmonic spectra measured in the experiment from the target molecule ($\vec{E}_{\text{HHG}}^{\text{mol}}$) and a reference atom ($\vec{E}_{\text{HHG}}^{\text{ref}}$). The reference atom should have the same ionization potential with the target molecule and known dipole moment ($\vec{d}^{\text{ref}}$). In the same laser field, the ratio between $A(\omega,\theta)$ of the molecule and the reference atom is reduced to an angle-dependent scaling factor $\eta(\theta)$ which is a constant [7,16,37]. A separate dedicated experiment could measure the θ dependence of the tunneling probability, which gives information for $\eta(\theta)^2$. Therefore, the relation among the dipole moments $\vec{d}^{\text{mol}}(\omega,\theta)$, $\vec{d}^{\text{mol}}(\omega,-\theta)$ and $\vec{d}^{\text{ref}}(\omega)$ satisfies

$$\frac{\vec{E}_{\text{HHG}}^{\text{mol}}(\omega,\theta)}{\vec{E}_{\text{HHG}}^{\text{ref}}(\omega)} = \frac{\eta(\theta)\,\vec{d}^{\text{mol}}(\omega,\theta) + \eta(-\theta)\,\vec{d}^{\text{mol}}(\omega,-\theta)}{\vec{d}^{\text{ref}}(\omega)}. \qquad (9)$$

Then using the relationship between the recollision angles, the dipole moment $\vec{d}^{\text{mol}}(\omega,\theta)$ and $\vec{d}^{\text{mol}}(\omega,-\theta)$ can be decomposed into a x' component and y' component and decoupled by

$$d^{\text{mol}}(\omega,\theta)\cos(\theta)\eta(\theta) + d^{\text{mol}}(\omega,-\theta)\cos(\theta)\eta(-\theta) = d_{x'},$$
$$d^{\text{mol}}(\omega,\theta)\sin(\theta)\eta(\theta) - d^{\text{mol}}(\omega,-\theta)\sin(\theta)\eta(-\theta) = d_{y'},$$
$$(10)$$

where

$$d_{x'} = \frac{E_{\text{HHG}x'}^{\text{mol}}(\omega,\theta)}{E_{\text{HHG}}^{\text{ref}}(\omega)}d^{\text{ref}}(\omega),$$

$$d_{y'} = \frac{E_{\text{HHG}y'}^{\text{mol}}(\omega,\theta)}{E_{\text{HHG}}^{\text{ref}}(\omega)}d^{\text{ref}}(\omega).$$

Then one can choose either $\vec{d}^{\text{mol}}(\omega,\theta)$ or $\vec{d}^{\text{mol}}(\omega,-\theta)$ to reconstruct the molecular orbital. Here we choose the $\vec{d}^{\text{mol}}(\omega,-\theta)$. Note that the dipole moments $\vec{d}^{\text{mol}}(\omega,\theta)$ and $\vec{d}^{\text{mol}}(\omega,-\theta)$ can be decoupled from Eq. (7) just because the electrons recollide with parent molecule from two noncollinear directions, and if the electrons recollide with parent molecule from two collinear directions, the dipole moments cannot be decoupled [21].

The AMOT is achieved in the molecular frame, so the dipole moment $\vec{d}^{\text{mol}}(\omega,-\theta)$ should be transformed into the molecular frame by utilizing the relationship between α, θ, and ϑ, i.e., $\vartheta + \theta = \alpha$ [see Fig. 2(b) and the discussion above]. Moreover, the AMOT requires one to obtain the dipole moments in all directions in the molecular frame. Therefore, high-order harmonic spectra when the molecule is oriented from $-\theta$ to $-\theta - 180°$ in the laboratory frame should be acquired. Correspondingly, the dipole moment $\vec{d}^{\text{mol}}(\omega,-\theta)$ from $0°$ to $-180°$ in the molecular frame can be obtained. [In the following we denote the dipole moment at ϑ in the molecular frame as $\vec{d}_{-\theta}^{\text{mol}}(\omega,\vartheta)$.] This ensures that the structure information of all directions can be obtained. For example as displayed in Fig. 3(c), the recollision angles of electrons are concentrated around $-14°$ and $14°$ in the laboratory frame. The dipole moment $\vec{d}^{\text{mol}}(\omega,-14)$ is used to reconstruct the molecule. While the molecule is oriented from $-14°$ to $-194°$ in the laboratory frame, the dipole moment $\vec{d}_{-14°}^{\text{mol}}(\omega,\vartheta)$ will scan the molecule from $0°$ to $-180°$ in the molecular frame.

To reconstruct the target molecular orbital in the molecular frame, the dipole moments $\vec{d}_{-14°}^{\text{mol}}(\omega,\vartheta)$ obtained in different orientation angles need to be projected on the y and x axis in the molecular frame. The projections on y and x axis are $d_y^L(\omega,\vartheta)$ and $d_x^L(\omega,\vartheta)$. The dipole moments $d_y^L(\omega,\vartheta)$ and $d_x^L(\omega,\vartheta)$ rely on the transition between the continuum state and ground state and can be described as

$$d_y^L(\omega,\vartheta) = \langle\psi_0|y|e^{i[kx\cos(\vartheta)+ky\sin(\vartheta)]}\rangle$$
$$= \int dy\,\psi_0^* y e^{i[kx\cos(\vartheta)+ky\sin(\vartheta)]},$$
$$d_x^L(\omega,\vartheta) = \langle\psi_0|x|e^{i[kx\cos(\vartheta)+ky\sin(\vartheta)]}\rangle$$
$$= \int dx\,\psi_0^* x e^{i[kx\cos(\vartheta)+ky\sin(\vartheta)]}. \qquad (11)$$

Therefore, the orbital is reconstructed by the equation

$$\psi_y^L(x,y) = \frac{F_{k\to r}\big[d_y^L(\omega,\vartheta)\big]}{y}$$
$$= \frac{1}{y}\sum_\vartheta\sum_\omega d_y^L(\omega,\vartheta)\exp\{i[k\cos(\vartheta)x+k\sin(\vartheta)y]\},$$
$$\psi_x^L(x,y) = \frac{F_{k\to r}\big[d_x^L(\omega,\vartheta)\big]}{x}$$
$$= \frac{1}{x}\sum_\vartheta\sum_\omega d_x^L(\omega,\vartheta)\exp\{i[k\cos(\vartheta)x+k\sin(\vartheta)y]\}. \qquad (12)$$

Here $\psi_y^L(x,y)$ and $\psi_x^L(x,y)$ are the reconstructed orbital using the dipole moments projected on the y and x axis of the molecular frame. The detailed analysis of the molecular orbital tomography can be obtained from Ref. [7].

IV. RESULTS AND DISCUSSION

We select the harmonics H21 to H65 at 19 different orientation angles between $-14°$ and $-194°$ to reconstruct the HOMO of CO. Following the reconstruction procedure in Eq. (11), the HOMO of CO is reconstructed. The normalized
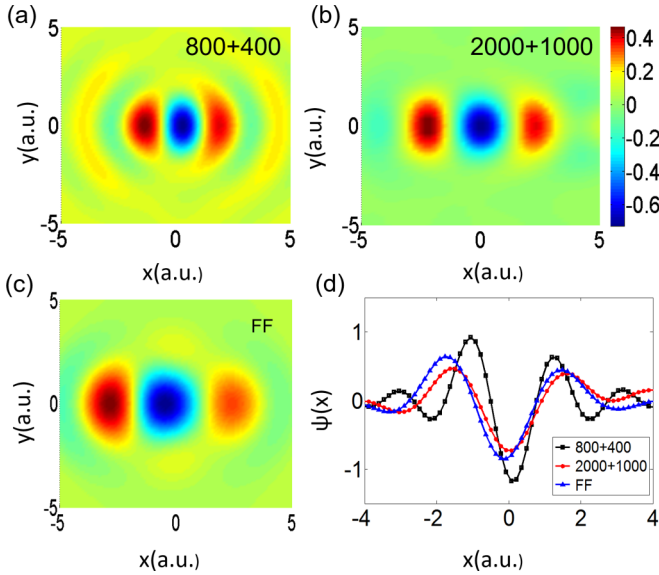
FIG. 5. (a) The reconstructed orbital of the HOMO of CO with the $800 + 400$ nm laser field. (b) The reconstructed orbital with the $2000 + 1000$ nm laser field. (c) The corresponding Fourier-filtered (FF) *ab initio* orbital. (d) Cuts along the $y = 0$ for the reconstructed orbital with the $800 + 400$ nm laser field (black curve), the reconstructed orbital with the $2000 + 1000$ nm laser field red curve) and the corresponding FF *ab initio* orbital (blue curve).
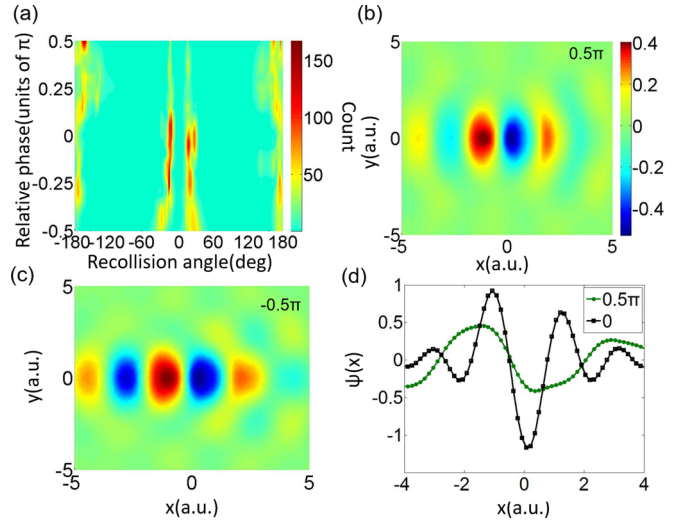

FIG. 6. (a) The count of the recollision electron as a function of relative phase and the recollision angles. (b) The reconstructed orbital with the 0.5π laser field. (c) The reconstructed orbital with the -0.5π laser field. (d) Cuts along the $y = 0$ for the reconstructed orbital with the 0.5π laser field (green curve) and the reconstructed orbital with 0 laser field (black curve).

real part of the reconstructed orbital with the Stark shift is presented in Fig. 5(a). Figure 5(c) is the corresponding Fourier-filtered (FF) *ab initio* orbital [38]. Comparing Fig. 5(a) with Fig. 5(c), one can see that the structure of the HOMO of CO is well reproduced with the two-color orthogonally polarized multicycle laser field. However, there are also some distortions such as the spatial diffusivity of the orbital and a shift of the reconstructed orbital. These distortions arise from the limited spectral range and the additional laser-induced Stark phase. Therefore, these distortions can be reduced by choosing a broad spectral range and an appropriate global phase. Figure 5(b) is the reconstructed orbital with the harmonics H31 to H160 and a slight global phase (-0.015π) [21] in a $2000 + 1000$ nm two-color orthogonally polarized laser field. Figure 5(d) shows the cuts along the $y = 0$ axis for the reconstructed orbital with the $800 + 400$ nm laser field (black curve), the reconstructed orbital with $2000 + 1000$ nm laser field (red curve), and the corresponding FF *ab initio* orbital (blue curve). Figures 5(b) and 5(d) show that these distortions are obviously reduced with the broader spectrum range. The structure of the HOMO of CO is much better reconstructed. These distortions have also been found and discussed in previous works [19,22]. In previous discussions, the reason of these distortions is the limitation of the spectrum range as well, and thus these distortions can be reduced with a wide spectrum.

Moreover, in Fig. 1, one can see that different relative phases will lead to different electron trajectories and recollision angles. Figure 6(a) shows the count of weighted numbers of recollision electron as a function of relative phase and the recollision angles when the intensity ratio of the two-color laser field is 1:10. It is shown that, in the range -0.5π to

-0.3π, the recollision angles are concentrated around $-14°$, $14°$, and $165°$. In the range -0.3π to -0.2π, recollision angles are concentrated around $-14°$, $14°$, $-165°$, and $165°$. When the relative phase is changed from -0.2π to 0.1π, the recollision angles are concentrated around $-14°$ and $14°$. When the relative phase is changed from 0.1π to 0.5π, the recollision angles are concentrated around $-165°$ and $165°$. As has been discussed above, to achieve AMOT, the electron should be manipulated to recollide with the parent molecule in two noncollinear angles (θ and $-\theta$). Therefore, only in the range -0.2π to 0.5π, the molecular orbital can be reconstructed.

In Figs. 6(b) and 6(c), we display the reconstructed orbitals when the relative phases of the two-color laser fields are 0.5π and -0.5π (the intensity ratio is 1:10 and the wavelength is 800 nm). It is found that, when the relative phase is 0.5π, the molecular orbital is reconstructed well. When the relative phase is -0.5π, the reconstructed orbital has apparent distortion. This is because the requirement for the recollision angles is not well satisfied in the relative phase of -0.5π. Figure 6(d) compares the cuts along $y = 0$ for the reconstructed orbitals with the relative phase of 0.5π (green curve) and 0 (black curve). One can see that the reconstructed orbital with the relative phase of 0.5π is spatially diffused comparing with that of 0. This is because, although the recollision angles of 0.5π satisfy the requirement for AMOT, the width of the recollision angle distribution is broader than that of 0, which will decrease the spatial resolution.

Figure 7(a) shows the recollision angle distribution as a function of intensity ratio ($I_{y'}/I_{x'}$) when the relative phase is 0. It is found that, with different intensity ratios, the recollision angles are still concentrated around $-14°$ and $14°$. With the intensity ratio increasing, the distribution of the recollision angles is narrower. When the intensity ratio is 1:1, the recollision angle distribution is very broad, which will lead
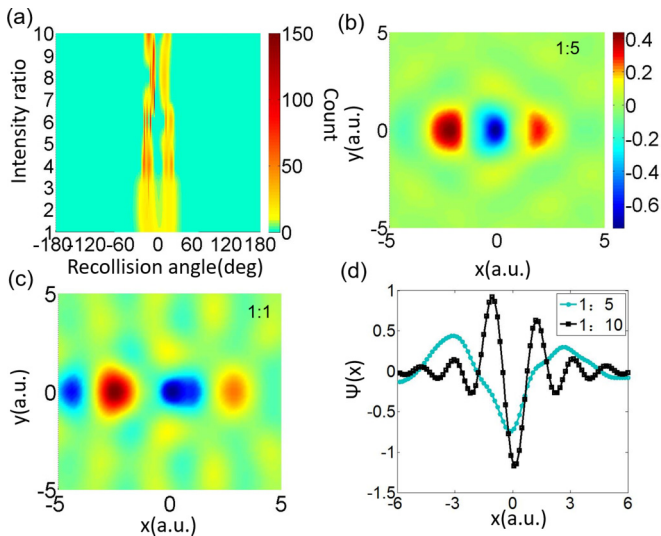
FIG. 7. (a) The count of the recollision electron as a function of intensity ratio $(I_{y'}/I_{x'})$ and the recollision angles. (b) The reconstructed orbital with a 1:5 laser field. (c) The reconstructed orbital with a 1:1 laser field. (d) Cuts along the $y = 0$ for the reconstructed orbital with the reconstructed orbital with a 1:5 laser field (cyan curve) and the reconstructed orbital with a 1:10 laser field (black curve).

FIG. 8. (a) The reconstructed orbital with the fluctuation of the relative phase from 0.1π to -0.1π. (b) Cuts along the $y = 0$ for the reconstructed orbital with the fluctuation of the relative phase (red curve), without the fluctuation of the relative phase (black curve) and corresponding FF *ab initio* orbital (blue curve). (c) The reconstructed orbital with the fluctuation of the intensity ratio by $\pm5\%$. (d) Cuts along the $y = 0$ for the reconstructed orbital with the fluctuation of the intensity ratio (cyan curve), without the fluctuation of the intensity ratio (black curve) and corresponding FF *ab initio* orbital (blue curve).

to a distortion of the reconstructed orbital [see Fig. 7(c)]. When the intensity ratio is increased to 1:5, the recollision angles are more concentrated, and the reconstructed orbital becomes more accurate [see Fig. 7(b)]. In Fig. 7(d) we compare the cuts along $y = 0$ for the reconstructed orbitals with the intensity ratio being 1:5 (cyan curve) and 1:10 (black curve). As the the width of the recollision angle distribution in the intensity ratio of 1:10 is narrower than that of 1:5, the reconstructed orbital is more accurate than that of 1:5.

V. INFLUENCE OF THE LASER PARAMETER FLUCTUATION

In a real experiment, the relative phase and intensity ratio are not precisely fixed. For a typical experiment, the fluctuation of the relative phase is around 0.1π and the fluctuation of the intensity ratio is around $\pm5\%$. In Fig. 8 we calculate the reconstructed orbital considering the fluctuation of laser field parameter. In Fig. 8(a) we calculate the high-order harmonics with the relative phase varying from -0.1π to 0.1π and sum them to obtain the total harmonics. Then the reconstructed orbital considering the fluctuation of the relative phase is obtained using the total harmonics. From Fig. 8(a) one can see that even the relative phase is fluctuated between -0.1π and 0.1π, and the molecular orbital can also be reconstructed well. From Fig. 6(a) it is shown that, in the range -0.1π to 0.1π the recollision angles are concentrated around $-14°$ and $14°$. As a result, when the relative phase is changed from -0.1π to 0.1π, the recollision angles do not have an obvious change. Therefore, the molecular orbital can also be reconstructed. In Fig. 8(b) we compare the cuts of the reconstructed orbital with the fluctuation of the relative phase, the reconstructed orbital without the fluctuation of the relative phase, and the
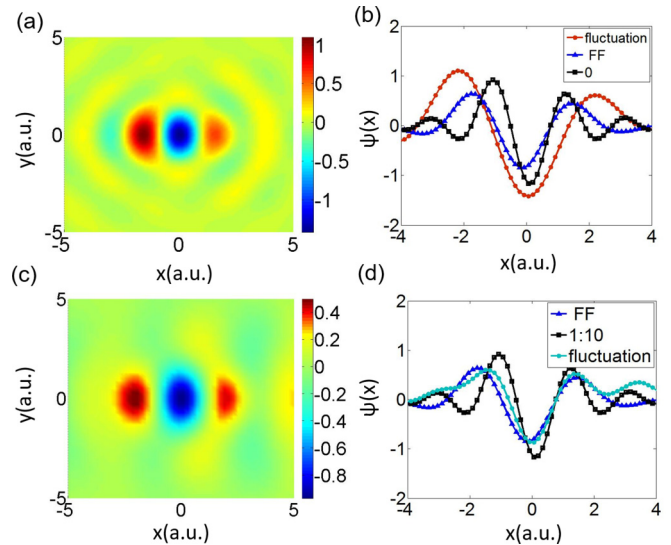
corresponding FF orbital. It is shown that, due to the fluctuation of the relative phase, the reconstructed orbital is spatially diffused. Figures 8(c) and 8(d) display the reconstructed orbital when the intensity ratio is fluctuated around 5%. It is found that, even when the fluctuation of the intensity ratio is taken into account, the molecular orbital can also be successfully reconstructed. This is because, as shown in Fig. 7(a), the recollision angles do not change significantly as the intensity ratio varies.

Our method also has some limitations. First, our method depends on the manipulation of the electron trajectories. Therefore, the relative phase of laser field should be controlled and stabilized. In Fig. 8 we have shown the influence of the fluctuation of laser parameters for our method. Although our method works well in a real case that the laser parameters change in a moderate range, if the fluctuation of the relative phase is very large, the molecular orbital cannot be reconstructed well. Second, our method requires the orientation of the molecule. However, for a three-dimensional molecule, it is hard to be oriented. Therefore, for a three-dimensional molecule our scheme cannot be easily carried out. Third, the result of AMOT depends on the range of the harmonic spectrum. As the spectrum of high order harmonics is limited, some detailed structures of molecular orbitals cannot be reconstructed in our method.

VI. CONCLUSION

We theoretically demonstrated a method for tomographic reconstruction of an asymmetric molecular orbital with

two-color orthogonally polarized multicycle laser pulses. Our scheme is based on two-dimensional manipulation of the electron trajectories, therefore it is insensitive to the angular dependence of the ionization rate in the external field and can avoid the negative effect induced by the Stark shift, which may make the AMOT unfeasible. In our scheme, the unidirectional recollision is independent from the molecular structure, and our scheme can be applied to various molecules. In addition, our scheme is insensitive to the fluctuation of

the laser parameters and can easily be carried out in the experiments.

[1] M. Drescher, M. Hentschel, R. Kienberger, G. Tempea, C. Spielmann, G. A. Reider, P. B. Corkum, and F. Krausz, Science **291**, 1923 (2001).

[2] Y. Mairesse, A. de Bohan, L. J. Frasinski, H. Merdji, L. C. Dinu, P. Monchicourt, P. Breger, M. Kovacev, R. Taïeb, B. Carré, H. G. Muller, P. Agostini, and P. Salières, Science **302**, 1540 (2003).

[3] Y. Li, M. Li, Y. Zhou, X. Ma, H. Xie, P. Lan, and P. Lu, Opt. Express **25**, 11233 (2017).

[4] D. Shafir, Y. Mairesse, H. J. Wörner, K. Rupnik, D. M. Villeneuve, P. B. Corkum, and N. Dudovich, New J. Phys. **12**, 073032 (2010).

[5] D. Shafir, Y. Mairesse, D. M. Villeneuve, P. B. Corkum, and N. Dudovich, Nat. Phys. **5**, 412 (2009).

[6] A. L'Huillier and P. Balcou, Phys. Rev. Lett. **70**, 774 (1993); S. A. Rezvani, Z. Hong, X. Pang, S. Wu, Q. Zhang, and P. Lu, Opt. Lett. **42**, 3367 (2017); L. Li, Z. Wang, F. Li, and H. Long, Opt. Quantum Electron. **49**, 73 (2017); L. Li, X. Zhu, P. Lan, L. He, and P. Lu, arXiv:1702.04084v1.

[7] S. Haessler, J. Caillat, and P. Salières, J. Phys. B **44**, 203001 (2011).

[8] P. Saliéres, A. Maquet, S. Haessler, J. Caillat, and R. Taïeb, Rep. Prog. Phys. **75**, 062401 (2012).

[9] A. Tong, Y. Zhou, and P. Lu, Opt. Quant. Electron **49**, 77 (2017).

[10] H. J. Wörner, J. B. Bertrand, D. V. Kartashov, P. B. Corkum, and D. M. Villeneuve, Nature (London) **466**, 604 (2010).

[11] E. Hijano, C. Serrat, G. N. Gibson, and J. Biegert, Phys. Rev. A **81**, 041401 (2010).

[12] X. Liu, P. Li, X. Zhu, P. Lan, Q. Zhang, and P. Lu, Phys. Rev. A **95**, 033421 (2017).

[13] S. Patchkovskii, Z. Zhao, T. Brabec, and D. M. Villeneuve, Phys. Rev. Lett. **97**, 123003 (2006).

[14] E. V. van der Zwan and M. Lein, Phys. Rev. Lett. **108**, 043004 (2012).

[15] X. Ma, M. Li, Y. Zhou, and P. Lu, Opt. Quantum Electron. **49**, 170 (2017).

[16] J. Itatani, J. Levesque, D. Zeidler, H. Niikura, H. Pápin, J. C. Kieffer, P. B. Corkum, and D. M. Villeneuve, Nature (London) **432**, 867 (2004).

[17] S. Haessler, J. Caillat, W. Boutu, C. Giovanetti-Teixeira, T. Ruchon, T. Auguste, Z. Diveki, P. Breger, A. Maquet, B. Carré, R. Taieb, and P. Saliéres, Nat. Phys. **6**, 200 (2010).

[18] C. Zhai, X. Zhu, P. Lan, F. Wang, L. He, W. Shi, Y. Li, M. Li, Q. Zhang, and P. Lu, Phys. Rev. A **95**, 033420 (2017).

[19] C. Vozzi, M. Negro, F. Calegari, G. Sansone, M. Nisoli, S. D. Silvestri, and S. Stagira, Nat. Phys. **7**, 822 (2011).

[20] Y. J. Chen, L. B. Fu, and J. Liu, Phys. Rev. Lett. **111**, 073902 (2013).

[21] E. V. van der Zwan, C. C. Chirilá, and M. Lein, Phys. Rev. A **78**, 033410 (2008).

[22] M. Qin, X. Zhu, Q. Zhang, and P. Lu, Opt. Lett. **37**, 5208 (2012).

[23] X. Zhu, M. Qin, Q. Zhang, Y. Li, Z. Xu, and P. Lu, Opt. Express **21**, 5255 (2013).

[24] H. Niikura, N. Dudovich, D. M. Villeneuve, and P. B. Corkum, Phys. Rev. Lett. **105**, 053003 (2010).

[25] H. Yun, K. M. Lee, J. H. Sung, K. T. Kim, H. T. Kim, and C. H. Nam, Phys. Rev. Lett. **114**, 153901 (2015).

[26] M. He, Y. Li, Y. Zhou, M. Li, and P. Lu, Phys. Rev. A **93**, 033406 (2016); H. Long, L. Bao, A. A. Habeeb, and P. Lu, Opt. Quantum Electron. **49**, 345 (2017).

[27] M. P. Minitti, J. M. Budarz, A. Kirrander, J. S. Robinson, D. Ratner, T. J. Lane, D. Zhu, J. M. Glownia, M. Kozina, H. T. Lemke, M. Sikorski, Y. Feng, S. Nelson, K. Saita, B. Stankus, T. Northey, J. B. Hastings, and P. M. Weber, Phys. Rev. Lett. **114**, 255501 (2015).

[28] N. B. Delone and V. P. Krainov, J. Opt. Soc. Am. B. **8**, 1207 (1991).

[29] X. Zhang, X. Zhu, X. Liu, D. Wang, Q. Zhang, P. Lan, and P. Lu, Opt. Lett. **42**, 1027 (2017).

[30] X. M. Tong, Z. X. Zhao, and C. D. Lin, Phys. Rev. A **66**, 033402 (2002).

[31] M. Lewenstein, P. Balcou, M. Y. Ivanov, A. L'Huillier, and P. B. Corkum, Phys. Rev. A **49**, 2117 (1994).

[32] A. Etches, M. B. Gaarde, and L. B. Madsen, Phys. Rev. A **86**, 023818 (2012).

[33] G. L. Kamta and A. D. Bandrauk, Phys. Rev. A **71**, 053407 (2005).

[34] B. K. McFarland, J. P. Farrell, P. H. Bucksbaum, and M. Göhr, Science **322**, 1232 (2008).

[35] X. Zhou, R. Lock, N. Wagner, W. Li, H. C. Kapteyn, and M. M. Murnane, Phys. Rev. Lett. **102**, 073902 (2009).

[36] P. Dietrich, N. H. Burnett, M. Ivanov, and P. B. Corkum, Phys. Rev. A **50**, R3585 (1994).

[37] M. Qin and X. Zhu, Opt. Laser Technol. **87**, 79 (2017).

[38] M. J. Frisch, Gaussian 03, Revision C.02 (Gaussian, Wallingford, CT, 2010).